A&A 533, A137 (2011)
DOI: 10.1051/0004-6361/201116860

Astronomy & Astrophysics

H_2 flows in the Corona Australis cloud and their driving sources⋆

M. S. N. Kumar[1], S. Sharma[2,5], C. J . Davis[3,4], J. Borissova[2], and J. M. C. Grave[1]

[1] Centro de Astrofísica da Universidade do Porto, Rua das Estrelas, 4150-762 Porto, Portugal
[2] Departamento de Física y Astronomía, Facultad de Ciencias, Universidad de Valparaíso, Ave. Gran Bretaña 1111, Playa Ancha, Casilla 53, Valparaíso, Chile
[3] Joint Astronomy Center, 660 N. A'ohoku Pl, Hilo, Hawaii 96720, USA
[4] NASA Headquarters, Science Mission Directorate, 300 E St SW, Washington, DC 20546, USA
[5] Aryabhatta Research Institute of Observational Sciences, Nainital 263129, India
e-mail: nanda@astro.up.pt

Received 9 March 2011 / Accepted 2 August 2011

ABSTRACT

Aims. We uncover the H_2 flows in the Corona Australis molecular cloud and in particular identify the flows from the Coronet cluster.
Methods. A deep, near-infrared H_2 v = 1–0 S(1), 2.122 μm-line, narrow-band imaging survey of the R CrA cloud core was carried out. The nature of all candidate-driving sources in the region was evaluated using data available from the literature and also by fitting the spectral energy distributions (SED) of each source either with an extincted photosphere or YSO model. Archival *Spitzer*-IRAC and MIPS data was used to obtain photometry, which was combined with USNO, 2MASS catalogs and millimeter photometry from the literature, to build the SEDs. We identify the best candidate-driving source for each outflow by comparing the flow properties, available proper motions, and the known/estimated properties of the driving sources. We also adopted the thumbrule of outflow power as proportional to source luminosity and inversely proportional to the source age to reach a consensus.
Results. Continuum-subtracted, narrow-band images reveal several new Molecular Hydrogen emission-line Objects (MHOs). Together with previously known MHOs and Herbig-Haro objects we catalog at least 14 individual flow components of which 11 appear to be driven by the R CrA aggregate members. The flows originating in the Coronet cluster have lengths of ~0.1–0.2 pc. Eight out of nine submillimeter cores mapped in the Coronet cluster region display embedded stars driving an outflow component. Roughly 80% of the youngest objects in the Coronet are associated with outflows. The MHO flows to the west of the Coronet display lobes moving to the west and vice-versa, resulting in nondetections of the counter lobe in our deep imaging. We speculate that these counter flows may be experiencing a stunting effect in penetrating the dense central core.
Conclusions. Although this work has reduced the ambiguities for many flows in the Coronet region, one of the brightest H_2 feature (MHO2014) and a few fainter features in the region remain unassociated with a clear driving source. The flows from Coronet, therefore, continue to be interesting targets for future studies.

Key words. stars: formation – ISM: jets and outflows – stars: variables: T Tauri, Herbig Ae/Be – Herbig-Haro objects

1. Introduction

The Corona Australis molecular cloud (see the review by Neuhauser & Forbich 2008), located in the southern hemisphere of the sky, is one of the nearest (130–170 pc; recommended value is 130 pc) and best studied star-forming regions with intense star formation activity. The 1.2 mm dust continuum emission, mapped by Chini et al. (2003) using the SIMBA array on the SEST telescope, provides a good representation of the dense regions of this cloud where most of the active star formation takes place. The densest region of this cloud roughly coincides with the Herbig Ae/Be star R Corona Austrinae (RCrA), surrounded by a cluster of young stars, well-known as the Coronet cluster (Taylor & Storey 1984). The Coronet cluster and associated molecular core has been the target of several studies at different wavelengths, from X-rays (for a complete list, see the review by Neuhauser & Forbich 2008) through the optical and infrared (Wilking et al. 1997) to the submillimeter (submm) (Nutter et al. 2005).

Outflows and jets are ubiquitous phenomena associated with star formation activity. Bipolar outflows are unambiguously identified by mapping the two lobes using molecular line transitions from species such as CO or SiO at (sub)mm wavelengths. Observations of optical Herbig-Haro (HH) objects and/or near-infrared (near-IR) H_2 v = 1–0 S(1) line emission features often complement these radio data; indeed, they can be more successful in tracing the flow components, particularly in crowded regions, because of the higher spatial resolution typically available at these shorter wavelengths.

Molecular line maps of the Coronet region show a prominent east-west bipolar outflow and a weak north-south flow (Anderson et al. 1997; Groppi et al. 2004, 2007). The east-west flow is thought to be driven by sources around IRS7, which is located roughly 15–20″ southeast of RCrA. The weak north-south flow is driven by the IRS1 source. This outflow is associated with HH 100, and its driving source is often referred to as HH100-IR. In contrast, at least 20 HH objects are known to be located in the close vicinity of the Coronet cluster (see Wang et al. 2004, and references therein). These data suggest the presence of several flow components. The east-west molecular outflow has been mapped in a number of molecular lines (e.g. CO, HCO+, and

⋆ Figure 1 is available in electronic form at http://www.aanda.org

SiO), and these observations likewise infer the presence of more than one outflow component (Anderson et al. 1997; Groppi et al. 2004). However, decomposition of these flow components has not been possible using the lower spatial resolution radio data.

The optical observations of Wang et al. (2004) and, more recently, the near-infrared H_2 images of Caratti o Garatti et al. (2006) and Peterson et al. (2011) provide a far superior view of outflow activity in the region. Even so, the concentration of candidate driving sources within a small region in the Coronet cluster, together with the large number of flow components, has made it difficult to unambiguously associate the flows with their driving sources. The rather complete census of the embedded population of young stars in the region uncovered by the new X-ray (Forbrich & Preibish 2007) and *Spitzer* Space Telescope observations (Currie & Sicilia-Aguilar 2011; Peterson et al. 2011) has prompted a fresh look at this region.

In an attempt to effectively trace the outflow activity in this region, we have conducted a deep H_2 $v = 1$–0 S(1) 2.12 μm narrow-band imaging survey of the northern part of the Corona Australis cloud. Many new Molecular Hydrogen emission-line Objects (MHOs Davis et al. 2010) are discovered from the new data, increasing the number of known flow components. In this work, we present and organize all the new and previously known outflow components.

For this purpose we use the following strategy. It has been suggested that the outflow power (and therefore MHO activity) is directly proportional to the luminosity and inversely to the evolutionary stage of their driving sources (e.g. Bontemps et al. 1996). First, by using the available information in the literature and then by modeling the spectral energy distributions (SED) of candidate driving sources in the region, we obtain a handle on the luminosity (mass) and evolutionary stage (age). Combining this information with the known properties of the outflows, as stated above, we then disentangle the individual flows and attribute the best driving sources to each flow. We also use the information on the proper motions of many knots in this region presented by Peterson et al. (2011) to arrive at the best-case scenario.

2. Observations and data analysis

2.1. Narrow-band H_2 imaging

Near-infrared observations of the Corona Australis molecular cloud were carried out using the 4 m Vitor Blanco Telescope at the Cerro-Tololo Inter-American Observatory (CTIO) on the nights of 11 to 13 July 2009. Imaging observations in the H_2 2.12 μm narrow-band filter and in the 2.2 μm broad-band K filter were obtained. These observations cover the northern part of dense gas regions traced by the 1.2 mm observations of Chini et al. (2003). The near-infrared wide-field camera ISPI, used to obtain the observational data, has a 10′ field of view and a plate scale of 0.3″ per pixel. A nine-point jitter pattern was used to obtain the observations, and the jitter sequence was repeated three times at each pointing of the telescope in each filter. An exposure of 60 s per jitter position was used for the H_2 observations, resulting in a total integration time of 27 min. For the K-band observations, the exposure time per jitter position was kept at 5 s, resulting in an integration time of 2 min.

Each set of jittered images were median combined to obtain a skyframe that was subtracted from each individual image. The sky-subtracted images were subsequently flattened by dividing by a smooth surface-fit obtained from the image. The individual exposures were co-added and mosaicked together using KAPPA and CCDPACK routines in the Starlink[1] suite of software.

2.2. Spitzer *photometry*

Archival *Spitzer* imaging data were used to obtain photometry of the sources in the Coronet region, which in turn were used for SED modeling. The data used correspond to the astronomical observational requests (AOR's) 3650816 and 17672960 (PI: G. Fazio) and 27041280 (PI: L. Allen). The BCD data in each of the four IRAC channels were corrected using artifact mitigation software provided by the *Spitzer* Science Center (SSC), and were then mosaicked together to obtain images corresponding to the region covered by our H_2 narrow-band observations. We used the *APPHOT* package in *IRAF* to obtain aperture photometry using an aperture of 2.4″ and a sky annulus of width 12″. The aperture corrections used for the Ch1-4 IRAC bands are 1.213, 1.234, 1.379, and 1.584.

MIPS 24 μm data of the same region were obtained from AOR 3664640 (PI: G. Fazio). The BCD data were mosaicked using standard templates available on MOPEX software. Aperture photometry was performed by using the MOPEX/APEX single frame template. Aperture size of 6″, sky annuli of width 7″ and an aperture correction factor of 2.05 were used.

3. Spectral energy distributions and modeling

As mentioned in the last paragraph of Sect. 1, we will first obtain the information on luminosities (masses) and evolutionary states (ages) of candidate driving sources in the Coronet region. For this purpose, we first searched the literature to obtain the information derived from standard methods. When such information was not available, particularly for the candidate sources that are well-detected in the *Spitzer* observations, we analyzed their spectral energy distribution by modeling. By SED fitting, we first eliminated sources that display redenned photospheres and then used the SED modeling to make a relative comparision of YSOs based on the fitted parameters (class, luminosity, and accretion rates) to select the most probable driving source for each identified outflow.

To this end we first built the SEDs of sources that appear to be associated with outflows and model these with a popular SED fitting tool (Robitaille et al. 2007). Not all SEDs are uniformly populated with the same photometric data because many of the millimeter sources are too bright (saturated) in the infrared bands. Some sources are resolved by optical and/or near-IR data and unresolved in the millimeter bands. Also, while we modeled all candidate driving sources in the mapped region, our focus is on a selected group of sources, which appear to drive outflows (see Table 2). These sources are prominently infrared-millimeter visible and were all modeled with 4–6 "data points" and with 1–6 upper or lower limits. The photometric data, apertures used, and the source of the data are listed in Table 1. Only the IRAC and MIPS photometry are independently derived by us, and the remaining photometric fluxes and errors are directly obtained from the references listed in Table 1. The apertures listed in Table 1 are those used for SED fitting and not necessarily the one with which photometry was obtained. This is because the SED fitter requires that the modeled source should not be larger than the aperture used for fitting. If a source is saturated in any band, the flux is assumed to be a lower limit and if the source

[1] http://starlink.jach.hawaii.edu

Table 1. Data used for SED fitting.

Band	Aperture	Reference
USNO B, R, I	3″	
2MASS J, H, K	2.4″	
Spitzer IRAC	3″	this work
Spitzer MIPS 24 μm	6″	this work
Spitzer MIPS 70 μm	9″	this work
450 μm SCUBA	8″	Nutter et al. (2005)
850 μm SCUBA	14″	Nutter et al. (2005)
1.2 mm SIMBA	24″	Chini et al. (2003)
1.1 mm SMA	3″	Groppi et al. (2007)

is too faint or larger than the aperture used, then the flux is assumed to be an upper limit. The 2MASS magnitudes are used as an upper limit if either the confusion flag was not "0" (implying confusion or extended source) or if the photometric quality flag was not the best (anything other than A). Ten percent errors are assumed for fluxes for the shorter wavelength bands (up to 8 μm) and 20% errors were used for all other longer wavelength data. In most cases, the photometric accuracy is better than the assumed error.

The resulting SED data were fed into the online SED fitting tool described by Robitaille et al. (2007). The distance and extinction values were allowed to vary in the range 130–170 pc and 5–45 A_v respectively. The SED fitting tool attempts to fit the observed fluxes, either with an extincted photosphere or an young stellar object (YSO). Models are constrained by the goodness of fit, χ^2. The YSO models used were obtained from a grid of 200 000 models, as described by Robitaille et al. (2006). Following the recommendations by Robitaille et al. (2007), only models that satisfy the criteria $\chi^2_{\rm best} - \chi^2 \leq 3$ per data point, where $\chi^2_{\rm best}$ is for the best-fit model, are used in estimating representative values of some physical parameters. These are essentially the group of models displayed in Fig. 4. The results using this group of models are listed in Table 3. The minimum, maximum, and weighted means (weights being the inverse of χ^2) are listed. It should be noted that the weighted means represent the parameter value distribution better than the difference in the maximum and minimum values. This is because even a single outlier model or parameter within the chosen χ^2 criteria can produce a minimum and a maximum that are not representative of the overall distribution. The minimum and maximum values nevertheless represent the extreme values for a given parameter from the group of models shown in Fig. 4. The evolutionary stage of Class 0/I quoted in Table 3 represents a fitted source age in the range 1–10 $\times$ 10^4 yrs.

In what follows we present the results from this procedure only for a few selected sources, for which the data available in the literature were not decisive in associating with detected MHOs. SEDs that were fitted with extincted photospheres are also not shown, except for one example, IRS11 (see Fig. 4), as they were ruled out of qualifying as driving sources.

4. The molecular hydrogen emission-line objects (MHOs)

Figure 1 (online only) is a color composite generated by using the *Spitzer* IRAC-4.5 μm image as red, the H_2 narrow-band image as green and the SII narrow-band image (mosaicked using archival ESO data from Wang et al. (2004) as blue. The SII data do not cover the lower portion of the image. The scaling of the individual images is adjusted to effectively display the embedded sources and the outflow components simulatneously. Since [SII] and H_2 trace different gas excitation conditions, they are often hugely complementary when one is trying to trace large sections of a protostellar outflow and/or connect outflow features with distant driving sources.

The continuum subtracted H_2 image of the mapped region is displayed in Fig. 2 where five groups of MHOs are marked by ellipses. The majority of the MHOs are contained within the large central ellipse. In Table 2 we list the positions of the MHOs and the identified driving sources, along with the measured flow lengths in arcseconds. Of these, the newly detected MHOs 2005, 2007, 2014, and 2017 are located away from the Coronet cluster and the dense core associated with it. The MHO features in the central region, corresponding to the Coronet cluster, are shown in Fig. 3.

The Coronet region is composed of many previously known infrared sources plus new infrared counterparts for the millimeter sources (Forbrich & Preibish 2007; Currie & Sicilia-Aguilar 2011; Peterson et al. 2011). Notably, SMM4, SMA1, and SMM2 have been recently detected by *Spitzer* images. This demonstrates that these submm cores are protostellar in nature. Furthermore, the SMA observations by Groppi et al. (2007) and Peterson et al. (2011) that provide millimeter fluxes are very useful in identifying the nature of the youngest protostars in the Coronet region. To disentangle each MHO flow and associate it with the best candidate driving source, we used the results of our SED modeling of all *Spitzer*-IRAC detected point sources (shown using circular symbols in Fig. 3) and utilized the proper motion information provided by Peterson et al. (2011). Together, these data have significantly improved the association of driving sources to the detected MHOs in the Coronet region. In Fig. 4 we show the observed SED data and the fitted models for candidate driving sources. The results of our SED modeling are presented in Table 3. In the following, we first discuss MHO features that have driving sources reasonably well identified.

4.1. MHOs with identified driving sources

MHO 2000/HH 99 – SMA2: MHO2000 is the brightest, well-collimated bow shock feature to the north of Coronet, associated with HH99. The suggestions of Wang et al. (2004) that it is driven by IRS6, and of Davis et al. (1999) that it is driven by IRS9 were ruled out by Caratti o Garatti et al. (2006) based on the evolved nature of IRS6 and also on the position angle of proper motion vectors. Recently, Peterson et al. (2011) suggest that it is driven by IRS7 or CXO34. The position angle of the proper motion vector for MHO2000 was found to be $39 \pm 6°$ by Caratti o Garatti et al. (2006) and $43 \pm 6°$ by Peterson et al. (2011). These position angles of the proper motion vectors clearly point towards the sources SMA2, IRS7, and CXO34.

Since MHO2000 is a bright and well-collimated feature, we assume that it has to be driven by a Class 0/I type object in the region. SMA2 is bright at millimeter wavelengths, very bright (nearly saturated) at 24 μm, and not detected at 8 μm IRAC images, therefore, has insufficient data points to be modeled. Nevertheless, the above characteristics are strong enough to classify it as a Class 0 protostar (see also Groppi et al. 2007; Peterson et al. 2011). In contrast, IRS7A display characteristics of being more evolved than SMA2 since it is bright at 8μm, not detected at (sub)millimeter, and also modeled to have a very low disk mass (0.004 $M_\odot$). Similarly, CXO34 is modeled as a substellar object with very low disk mass as well. In fact, using the SMA nondetections (both IRS7A and CXO34), Peterson et al. (2011) suggest an upper limit of only a few Jupiter masses

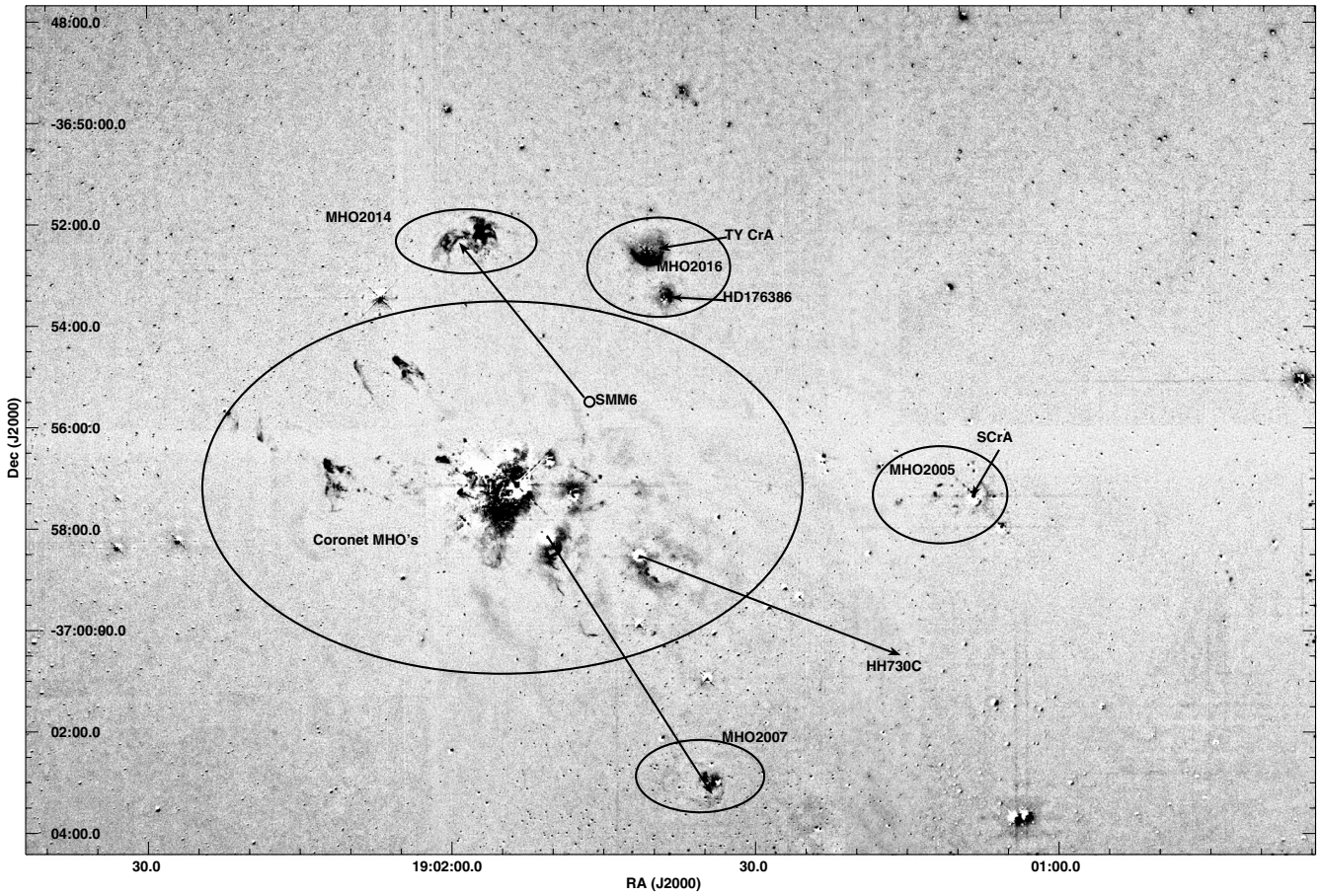

Fig. 2. Continuum-subtracted H_2 image of the mapped region, displayed with linear gray scales. Five groups of H_2 line emission features are marked by ellipses.

Table 2. MHO and source identifications and flow lengths.

MHO	RA (J2000)	Dec (J2000)	Length	Source	Comments
2000 A, B, C	19 02 04.8	–36 54 45	198″	SMA2	HH99 A, B, C
2001	19 02 01.00	–36 56 38	113″/145″	IRS6 or IRS5N	
2002	19 01 59.1	–36 57 17	70″	RCrA or CXO34	
2003, 2007, 2008	19 01 46.0	–37 00 06	350″	IRS1/HH100IR	HH96, HH97, HH100, HH101
2004	19 01 46.8	–36 56 55	64″	IRS6 and/or RCrA	HH104 (jet like)
2005 A, B	19 01 25.9	–36 57 20	258″	IRS5a/b	thin faint arc
2005, C, D, E...	19 01 15.6	–36 57 25	87″	SCrA	HH82 A, B
2006	19 01 39.2	–36 59 02	330″	IRS2	HH730 A, B, C
2008 D	19 01 40.0	–37 00 05	16″	Star1-100	1-100HH
2009	19 02 12.2	–36 56 43	193″	IRS7A	HH735, HH734
2011 D, E	19 02 12.2	–36 56 43	193″	SMA1/IRS7B	HH735, HH734
2011 A, B, 2012	19 02 20.6	–36 55 55	275″	SMM2	faint bow shocks
2013	19 02 09.2	–36 54 53.0	289″	T CrA	northern lobe, HH733 (bowshock)
2015	19 01 55.7	–36 58 42	67″	T CrA	southern lobe bowshock
2014	19 01 57.5	–36 52 12	236″	SMM6/MMS10-11 ?	HH732
2016	19 01 39.5	–36 53 02	–	TYCrA and HD176356	–

for the disk in these sources. On the contrary, they estimate a disk mass of 0.063 $M_\odot$ for SMA2, higher by a factor of ten. Therefore, we conclude that SMA2 drives the MHO2000 flow, which is a bright, well-collimated bowshock.

MHO 2003, 2008 (2007?) – IRS1/HH100IR: The source IRS1, also known as HH 100IR is known to drive the Herbig-Haro objects HH 100 and HH 97 (Wang et al. 2004). Caratti o Garatti et al. (2006) discovered MHO 2003 (an arc and an elongated knot) associated with IRS1. The deeper images presented here and by Peterson et al. (2011) reveal a new knot named as MHO2008, which is probably the tip of the flow associated with IRS1. While MHO2003 and MHO2008 are certainly driven by IRS1, it is likely that this flow is much longer that it terminates in MHO2007 (see the description of this MHO in the next subsection). MHO2003 appears to have a wide opening angle, MHO2009 from IRS2 and the confused flows from RCrA being the only two other cases in the region with large opening angles. Nisini et al. (2005) estimate a spectral type of K-M for the star, however, they point out that IRS1 and IRS2 are the only two

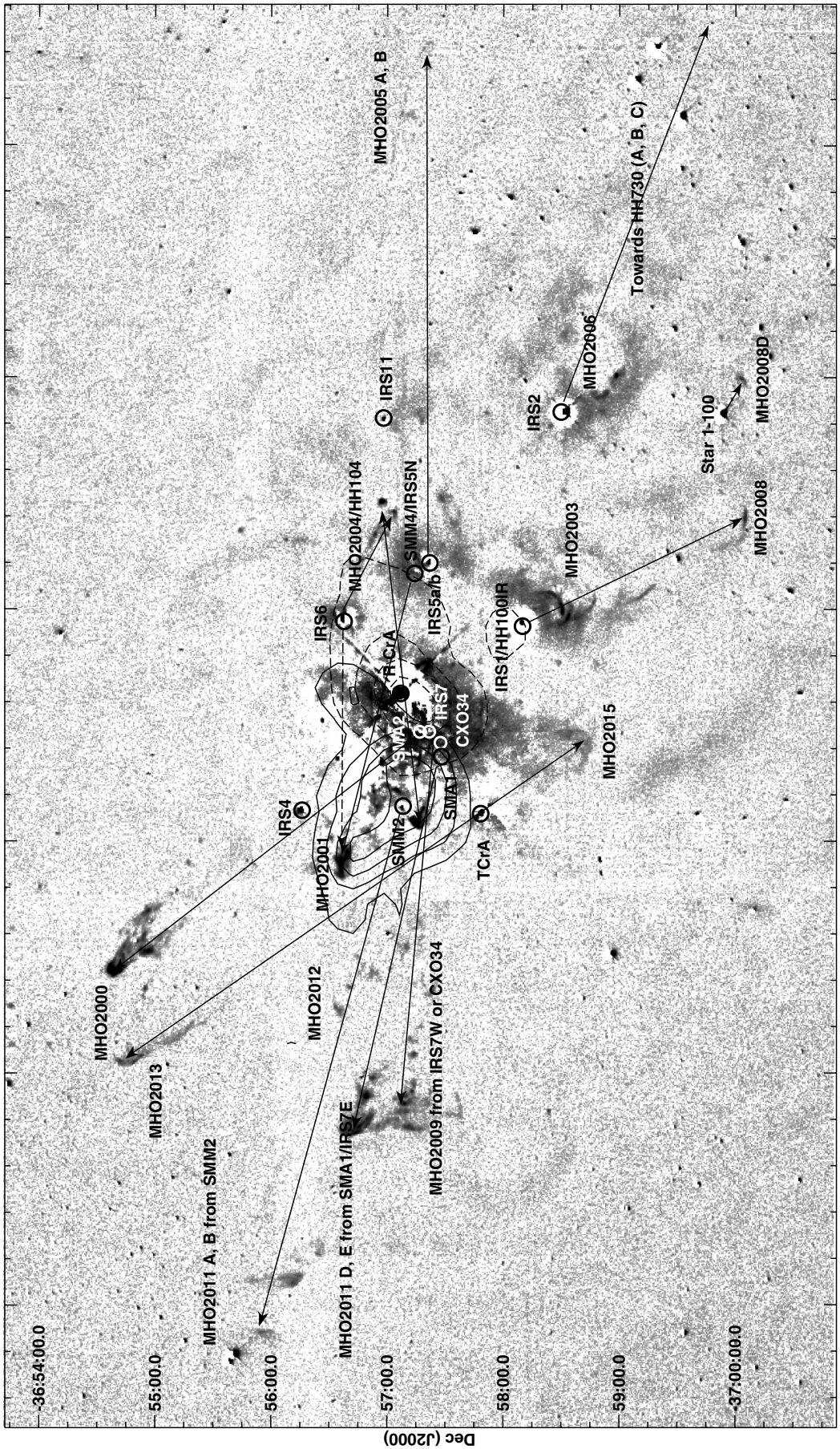

Fig. 3. Continuum-subtracted H_2 image of the Coronet subregion displayed using a logarithmic scaling. The circular symbols show all sources detected by the *Spitzer* IRAC images. The identifications are reproduced from Wilking et al. (1997) (IRS), Groppi et al. (2007) (SMA), and Nutter et al. (2005) (SMM). The arrows join the probable driving source with the corresponding MHO. When two arrows originate in the same source, it implies both outflow lobes are visible. The CO bipolar outflow mapped by Groppi et al. (2004) is shown by solid (blue lobe) and dotted (red lobe) contours. For the sake of clarity, MHO 2000, which is situated close to SMM2, is not marked in this figure.

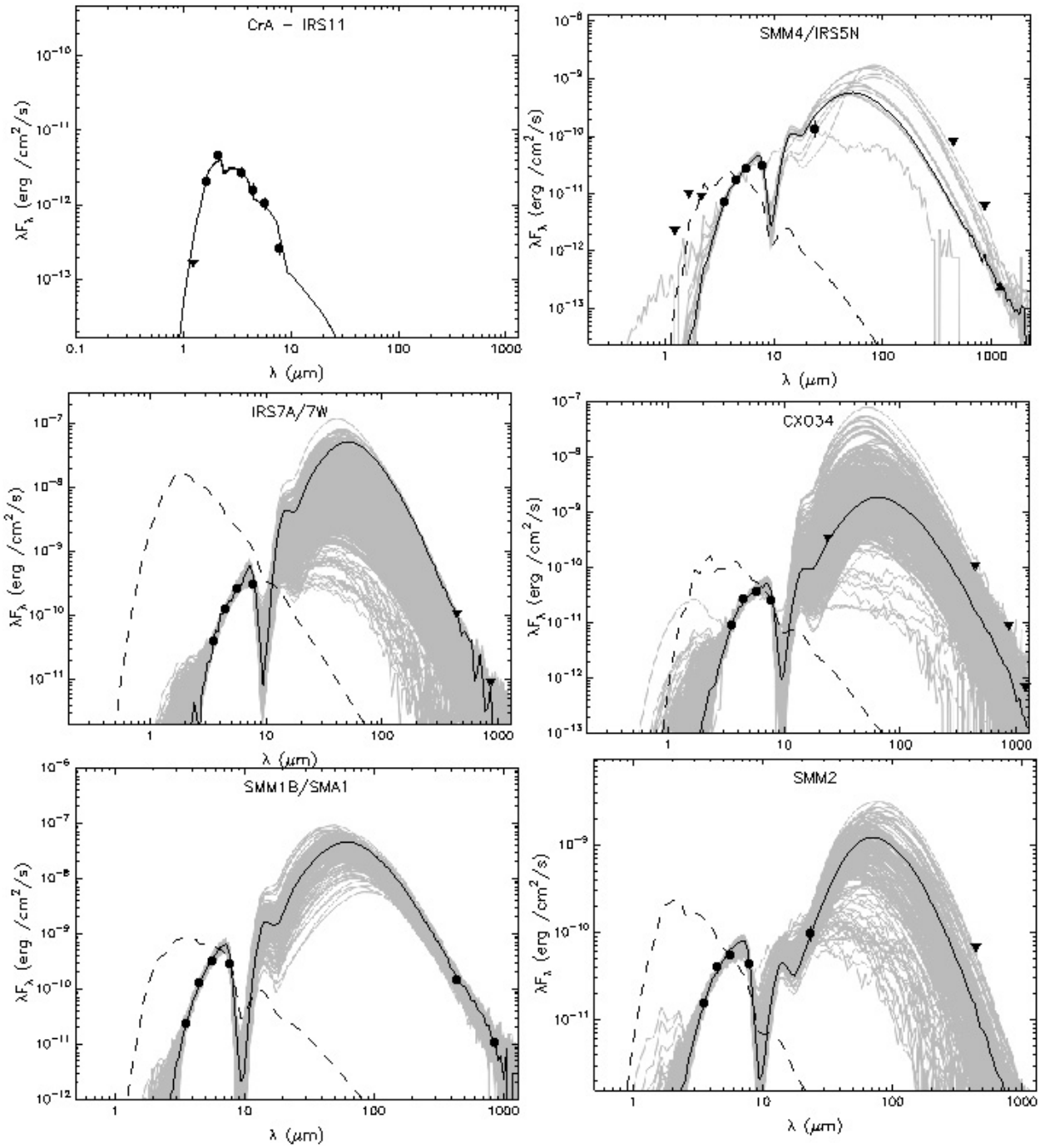

Fig. 4. The observed SEDs and their best-fit models. *Top left panel* shows an example of an extincted photosphere while the rest are YSOs. Circular symbols represent the data points, upward-facing triangles are lower limits and downward facing triangles are upper limits. The dashed line corresponds to the stellar photosphere model used in the best YSO model fit. The gray lines show the models that satisfy the χ^2 criteria described in the text. For the source IRS5N, the SMA data by Peterson et al. (2011) is additionally used in the SED fitting.

Table 3. SED-fitted parameters of selected sources in the Coronet.

Source	Class	L $\log(L_\odot)$	M_* $M_\odot$	$\dot{M}_{\rm disk}$ $\log(M_\odot\ yr^{-1})$	$M_{\rm disk}$ $\log(M_\odot)$
IRS5N/SMM4	0/I	–0.2, 1.8, (0.2)	0.1, 2.9, (0.5)	–8.9, –6.0, (–7.3)	–3.8, –1.6, (–2.2)
IRS7A/7W	0/I	0.1, 2.8, (1.1)	0.1, 6.8, (1.2)	–9.9, –4.7, (–7.0)	-4.1, –0.4, (–2.4)
CXO34	0/I	–0.4, 2.5, (0.4)	0.1, 6.5, (0.5)	–11.8, –5.2, (–8.0)	–5.0, –0.8, (–2.8)
SMA1	0/I	1.0, 2.9, (1.9)	0.2, 8.0, (3.3)	–9, –4.6, (–6.9)	–3.8, –0.5, (–1.7)
SMM2	0/I	–0.3, 2.0, (0.4)	0.1, 4.2, (0.7)	–10.5, –6.4, (–8.1)	–4.4, –1.3, (–2.8)

Notes. For each parameter, the minimum, maximum, and weighted mean (inside parantheses), selected by the χ^2 criteria discussed in the text are displayed. These values represent the group of models shown with gray lines in Fig. 4. SMM identifications are from Nutter et al. (2005), IRS identifications from Wilking et al. (1997), SMA identifications are from Groppi et al. (2007), and CXO identification is from Forbrich & Preibish (2007).

sources with a bolometric luminosity that is 60–80% higher than the stellar luminosities. Also, using Brackett line characteristics, they suggest it probably originates in an expanding stellar wind rather than in accreting regions. The arc-shaped MHO feature 2003 may therefore be due to fluorescence rather than due to a large opening angle of the flow.

MHO 2005 C, D, E–S CrA: This group of MHO knots represents the H_2 counterpart of the well-known optical features HH 82A, HH 82B, and HH 729A, B, C (Wang et al. 2004), which are located near the bright T-Tauri star S CrA. This star coincides with the millimeter peak MMS1 described by Chini et al. (2003). Previous studies have suggested that these HH objects are driven by S CrA (Reipurth & Graham 1988; Wang et al. 2004), and so are these MHO knots. The knots MHO2005A, B (Peterson et al. 2011) are not associated with S CrA, and is probably driven by IRS5a/b as discussed in Sect. 4.2.

MHO 2006/HH 730–IRS2: This source, first identified by Wilking et al. (1997), is classified as a young star with a mass of 1.4 $M_\odot$ by Nisini et al. (2005). The recently discovered MHO 2006 feature (Peterson et al. 2011) is clearly associated with this source and has a wide opening angle, most likely due to reasons like those discussed above with respect to IRS1. The HH objects HH 730A, HH 730B, and HH 730C, which terminate in a well-defined bowshock, clearly align with this source. We therefore associate HH 730 and the newly detected MHO 2006 object with a single flow driven by IRS2.

MHO 2011 A, B & 2012 – SMM2: The newly discovered knots 2011 A, B, and the 2012 are located to the west of the Coronet cluster. It comprises a number of knots and arcs that probably form part of at least two bow shocks. This flow is well aligned with the embedded IR source associated with the submm peak SMM2. The SED modeling presented here indicates that the *Spitzer* detected infrared counterpart to SMM2 is a young low mass star of Class 0/I type (see Table 3).

MHO 2013/2015/HH733 – TCrA: The faint bowshock MHO 2013 (Davis et al. 1999) by the side of MHO2000 is the H_2 counterpart of the Herbig-Haro object HH 733. Wang et al. (2004) suggest that this flow is driven by TCrA. The newly discovered MHO 2015 is a clear bow-shock feature, lying to the south of TCrA, and it marks the southern lobe of the bipolar outflow originating from TCrA. This is probably the only unambiguously detected bipolar outflow traced by two complementing bow-shock features in the entire Coronet region. Meyer & Wilking (2009) adopt a spectral type of F0 for TCrA.

MHO2008D – Star1-100: The star identified as 1-100HH by Wang et al. (2004) is associated with a newly discovered faint H_2 knot that is labeled as MHO2008D by (Peterson et al. 2011). This is very likely an independent flow driven by this star.

MHO 2016: This MHO feature has two conical nebulae A and B centered on TY CrA and HD176386, respectively. MHO 2012A is an extended conical nebula, centered on the H_α emission star TY CrA. MHO 2012B is a relatively faint, localized emission on the binary pre-main-sequence star HD176386.

4.2. MHOs with ambiguous driving source associations

MHO 2001 – IRS6b, CXO34, IRS5N: MHO 2001 is one of the brightest features to the east of Coronet cluster, well immersed in the reflection nebula. There is much confusion in this area. Since it is one of the brightest MHO features, it should be driven by a relatively young object of Class 0/I type. However, it appears to be close to most of the candidate driving sources (unlike MHO2000 which is farther away). Peterson et al. (2011) quote CXO34 as a possible candidate driving this flow. However, the same authors quote a position angle of the proper motion vector at 81° for the bright knot MHO2001A, which when traced backwards, points more directly to IRS6 or roughly towards IRS5N (considering an average of the PA from all the knots associated with MHO2011). IRS6 is known to be a binary source with one young and one old component (Nisini et al. 2005). Following the proper-motion vectors, a likely scenario is that the younger object of this binary component drives MHO2001. Alternatively, MHO2001 could be driven by SMM4/IRS5N, which is a millimeter peak associated with a faint IR source, that is modeled as a very young substellar object. We also point out the low flux density of the SMA peak associated with IRS5N in comparison to SMA1 or SMA2 Peterson et al. (2011). We favor the scenario of MHO2001 driven by IRS6 rather than IRS5N because of the likely stunting effect discussed in Sect. 5

MHO 2002, 2004 – RCrA: RCrA is the principal component of the Coronet cluster. We associate the previously detected bow-shaped object MHO 2002 with RCrA (labeled "E" by Caratti o Garatti et al. 2006) and possibly a knot from within the group labeled MHO 2004. Together, these would delineate an east-west bipolar outflow. These knots appear as a bowshock from a relatively wide-angled wind. The morphology of these MHO features suggests a wide-angled, poorly collimated wind rather than a collimated outflow. RCrA is a bright source that is saturated in all of the *Spitzer* bands. These properties conform to the nature of RCrA as a Herbig Ae/Be star with an estimated mass of 5–10 $M_\odot$ (Tuthill et al. 2001). Recently, Kraus et al. (2009) have used the *Very Large Array (VLA)* Interferometer to study this source and find a disk that is oriented north-south, suggesting an east-west outflow. The proposed MHO associations with RCrA presented above are in good agreement with this scenario.

MHO 2004/HH 104 – IRS6b or RCrA: We associate HH 104 and MHO 2004 with a faint, jet-like feature that is located close to the source IRS6. Caratti o Garatti et al. (2006) suggest that IRS6 is too evolved to be driving a powerful outflow. In their high-resolution VLT data, Nisini et al. (2005) identify IRS6 as a binary system (IRS6a and IRS6b), and by using photometric data, show that IRS6b has a stronger H-K color than IRS6a. Our K band data also partially resolve this binary source. Therefore, the HH 104/MHO 2004 outflow is probably driven by the fainter – though redder – infrared source, dubbed IRS6b by Nisini et al. (2005). IRS6 is unresolved in the mid-IR and submm photometric data.

MHO2004 also contains a bright bow-like knot that indicates a proper motion vector moving to the west; therefore, it could just as well be due to RCrA flow. Given that RCrA is a Herbig Ae/Be type star, the outflow from such a star would be composed of strong stellar winds and contribute to poorly collimated flows composed of many knots and shock surfaces.

MHO 2005 A, B – IRS5a/b: The bright infrared source IRS5 (Wilking et al. 1997) is found to be a subarcsecond binary source (Chen & Graham 1993; Nisini et al. 2005). The main component is labeled IRS5a by Nisini et al. (2005) and classified as a Class I source with low accretion activity. The faint, though well-defined, elongated MHO feature MHO 2016 (Fig. 3) that terminates in a small bow shock is aligned well with IRS5a. The Class I nature and the low accretion activity attributed to this source by Nisini et al. (2005) is consistent with the low brightness and morphology of MHO2016. Peterson et al. (2011) associate this feature with the prominent east-west CO flow. Although IRS11 (Wilking et al. 1997) is located along the same projected line as MHO 2016, it is unlikely to be the driving source since its SED represents a reddened photosphere. IRS11 is probably a reddened background star that is unrelated to the Coronet cluster.

MHO 2007 – IRS1/HH100IR: MHO 2007 is a group of knots discovered in the images of Peterson et al. (2011) and our H_2 images. Additionally, our deep H_2 data reveal a faint, but clear bow shock feature at the same location (see Fig. 1). The bright knots of MHO2007 are the H_2 counterparts of the HH objects HH 101A, B, N, and S. Peterson et al. (2011) associate this group of knots to the red lobe originating in IRS5N. Also, there is a star embedded in this group of MHO features /HH objects that was labeled Star30 by Hartigan & Lada (1985). Hartigan & Graham (1987) argued that Star30 is not the driving source for the HH 101 group of knots. From our SED fitting we concur with this viewpoint: using the USNO and 2MASS magnitudes we find that the photometry of star30 is best described by an extincted photosphere rather than a YSO. Hartigan & Lada (1985) and Hartigan & Graham (1987) suggest that HH 101 must be part of a long collimated outflow originating in HH 100IR (close to the Coronet cluster). The faint, but clear, bow-shock feature detected by our H_2 data could indeed be the terminating point of the flow from HH100IR. In Fig. 1, the tip of the arrow drawn from IRS1 points to the center of this bow-shock feature. Thus, the speculation of Hartigan & Graham (1987) and Hartigan & Lada (1985) can also represent a valid scenario. This flow from HH 100IR/IRS1 would then measure ~365″, corresponding to a single lobe length of ~0.23 pc. In such a case, HH 100IR/IRS1 may be driving a parsec scale outflow.

MHO2011 D, E – SMM1b/SMA1: The submm source identified by Nutter et al. (2005) as SMM1b and resolved as SMA1 by Groppi et al. (2007) appears as a point source in the *Spitzer*-IRAC images. The luminosity (see Table 4) of this source is relatively higher compared to other modeled sources in the region. The newly detected bow-shock features MHO 2011, D & E are well aligned with this source in projection. Further, the PA of the proper motion vector estimated by Peterson et al. (2011) points away from this source. The source SMM1c/SMA2 appears to be aligned with MHO 2011, but is a less probable option because: a) we have already shown that SMA2 very likely drives MHO2000, b) SMA1 is thought to be relatively older (a transitional Class 0/I object) than SMA2 (Class 0 protostar) (Groppi et al. 2007; Forbrich & Preibish 2007) (assuming a similar mass), therefore expected to be associated with a longer and relatively fainter flow. MHO2011, D, E therefore are best associated with SMA1.

MHO 2014 – SMM6: This is a bright extended H_2 feature, with a bow-like component (to the east; lefthand side in Fig. 2) and a clumpy component (western half). The bow-like components are associated with the previously known Herbig-Haro features HH 732 A, B, and C (Wang et al. 2004). These HH objects are not identified with any clear driving source. Peterson et al. (2011) compute the position angle (PA) for the proper motions to be in the range 31°–34° ± 15°and associate it with the blue lobe originating in IRS5N. They suggest MHO2007 as the red lobe of this flow. This scenario may appear likely, because MHO2007, MHO2014 and SMM4/IRS5N align along a straight line and SMM4 displays a peak at millimeter wavelengths. However, the 1.2 mm flux (and the resulting disk mass) of IRS5N, measured by the same authors, is weaker than sources such as SMA1 or SMA2. Furthermore, this source is visible in the infrared bands and is not very luminous. Our SED modeling suggests that SMM4/IRS5N is a substellar object with a luminosity ~0.5 $L_\odot$. These data together do not support the scenario of IRS5N driving a powerful, parsec scale outflow comprising of MHO2014 and MHO2007. It should also be noted that Peterson et al. (2011) associate SMM4 with IRS5 and state that the new peak detected using SMA observations is associated with IRS5N, while SMM4 and the new SMA peak are indeed the same, coinciding with IRS5N.

Here we propose SMM6 (MMS10-11) as an alternative driving source for MHO2014 (Nutter et al. 2005; Chini et al. 2003). Chini et al. (2003) note that there are no near-IR or FIR sources associated with MMS10-11 peaks. (Nutter et al. 2005) discard the proposition of Chini et al. (2003) that MMS6 is a deeply embedded protostar based on their interpretation of this source as a prestellar object. This interpretation may be valid, since the *Spitzer* MIPS 24 μm or 70 μm images do not reveal point-like or extended source associated with SMM6. However, the 160 μm emission in this region is bright and saturated, roughly following the morphology of the 850 μm emission from Nutter et al. (2005). Our supposition that SMM6 is the driving source for MHO2014 requires a PA of 41°, which is well within the value and error bars quoted by Peterson et al. (2011). Given that this is one of the brightest MHO in the region conforms to the proposition that it should be driven by a deeply embedded protostellar object invisible at the infrared wavelengths.

The western half (righthand side in Fig. 2) of MHO 2014 is very clumpy and not likely to be driven by a well-collimated Class 0 jet/outflow. The morphology of this clump and its location in the vicinity of the bright young stars TY CrA and HD 176386 may imply a different origin. TY CrA is a well known variable star of Orion type, and HD176386 is a pre-main-sequence double star coinciding with a submm peak (Chini et al. 2003). Lacking proper motion data, we therefore speculate that this clumpy knot might be due to an unidentified component of the TY CrA or due to the double components of HD176386.

5. Discussion

We discovered new MHO features tracing individual flows in the northern part of the Corona Australis region, which encompasses the Coronet cluster. Together with the previously known flow components, we have cataloged 16 individual flow lobes in the studied region (Table 1). Eleven of these flows are localized in the Coronet cluster region, which has a membership of about 14 stars that are detected in the x-ray (Forbrich & Preibish 2007) near-IR, mid-IR, FIR (*Spitzer*) (Peterson et al. 2011), and submm photometric data (Nutter et al. 2005; Groppi et al. 2007; Peterson et al. 2011). Thus, roughly 80% or more of the embedded sources in the Coronet cluster display an active outflow component. The region mapped in H_2 here is roughly similar to the region covered by Forbrich & Preibish (2007) in the x-ray

and *Spitzer* data. These authors identify nine embedded objects (meaning Class 0/I and flat-spectrum sources) in this region. Together with the newly identified SMA sources (Groppi et al. 2007; Peterson et al. 2011), all of the embedded sources are associated with MHO flows.

If we compare the submm cores from Nutter et al. (2005) with the detected MHO flows in this region, all cores except SMM1A and SMM6 are associated with a detected infrared source driving an outflow. SMM1A and SMM6 are the two cores that these authors classified as prestellar, of which we associate SMM6 with MHO2014, even though no infrared source is detected with this core up to 24 μm . Therefore, the studied region contains one, or at most two, starless cores and eight protostellar cores, which implies roughly 10% of starless cores in the region. The Corona Australis core is therefore a good example of a young star-forming cluster, with a very high rate of detected outflow activity and young stars.

From Fig. 3, we can see that for each driving source, only one of the outflow lobes is traced either through H_2 emission or HH objects. T CrA is the only exception in this region, associated with two lobes identified with bow shock features. For all the other flows, the identified flow lobes are oriented in such a way that they are flowing in a direction away from the central dense core and entering the less dense medium. The outflow lobes flowing towards the central dense core is usually absent. The dense core in the Coronet cluster is roughly centered on the Herbig Ae/Be star RCrA (Chini et al. 2003). We can see from Fig. 3 that the flow lobes from the sources to the left (east) of RCrA are all moving towards the east or northeast, while their eastern/southeastern counter-lobes are not detected. The sources located to the right (west) of RCrA display a similar, complimentary behavior. It appears that the outflows driven by the young stars are "stunted" because of the increased power needed to penetrate the dense gas inside the core. In comparison, the flow from TCrA, which is orientated north-south and avoids the dense core, is bipolar. The dense core around Coronet is concentrated within a 3′–4′ diameter. Since the detected single lobe lengths surpass this value, even assuming different inclinations, the brightest bow shocks or knots from the counterlobes should have been detected in our deep H_2 images, if the "stunting" effect was not real. Comparing Coronet to NGC 1333, we can see further support of the likely "stunting" effect scenario. NGC 1333 is another nearby region with a high incidence of detected MHOs (see Davis et al. 2008, and references therein). In NGC 1333, MHOs are associated with bipolar lobes of multiple outflows, even in a relatively shallow survey of Davis et al. (2008). However, the dense cores are ordered along a curved filament with gaps of low density regions (see Figs. 3 and 7 of Walsh et al. 2007), and the bipolar outflows can be seen punching out roughly perpendicular to the filamentary axis. The MHOs detected in this region can then be verified by comparing with Fig. 5 of Davis et al. (2008). Therefore, we speculate that the higher extinction dense core, has an important effect on the optical and infrared detection of the flow lobes. Only the lobes moving away to the rarer medium produce significant H_2 emission resulting in good detections. This observational feature may be a qualitative indication of the lower density of the outflowing gas compared to the density of the natal dense cores in which they form. It may also demonstrate how the outflowing gas penetrates out into a region of least pressure.

The nature of driving sources and associated flows: It can be seen from Table 2 that more than half of the detected flows, in particular the flows originating from the Coronet, display a single lobe length of ≥200″. This implies projected total flow lengths of ≥0.1 pc for the bipolar outflows at a distance of 130 pc. By assuming roughly similar inclination angles to the observed flows, a canonical jet speed of 100 km s^{-1}, a flow length of 0.1 pc indicates a dynamical time scale of ∼1200 yr for the outflows. Since the molecular hydrogen flows are driven by YSOs in their early evolutionary stage and since roughly 80% of such identified members are located in the Coronet cluster and are driving H_2 flows, the cluster should be very young with an age ∼1 Myr. Meyer & Wilking (2009) have evaluated the masses and ages of the Coronet sources using near-infrared spectra and evolutionary models. They find an age spread of 0.3–3 Myr and masses in the range 0.2–2.5 $M_\odot$ for the young aggregate.

Acknowledgements. We thank Christopher Groppi for providing the CO data for overplotting in Fig. 3. Kumar is supported by a Ciência 2007 contract, funded by FCT/MCTES (Portugal) and POPH/FSE (EC). S.S. and J.B. are supported by FONDECYT No. 1080086, by the Ministry for the Economy, Development, and Tourism's Programa Inicativa Científica Milenio through grant P07-021-F, awarded to The Milky Way Millennium Nucleus and from Comitee Mixto ESO-GOBIERNO DE CHILE. S.S. received partial support from Center of Excellence in Astrophysics and Associated Technologies BASAL CATA PFB-06. This work is based in part on archival data obtained with the *Spitzer* Space Telescope, which is operated by the Jet Propulsion Laboratory, California Institute of Technology under a contract with NASA. Support for this work was provided by an award issued by JPL/Caltech.

References

Anderson, I. M., Harju, J., Knee, L. B. G., & Haikala, L. K. 1997, A&A, 321, 375
Bontemps, S., André, P., Tereby, S., & Cabrit, S. 1996, A&A, 311, 858
Caratti o Garatti, A., Giannini, T., Nisini, B., & Lorenzetti, D. 2006, A&A, 449, 1077
Chen, W. P., & Graham, J. A. 1993, ApJ, 409, 319
Chini, R., Kampgen, K., Reipurth, B., et al. 2003, A&A, 409, 235
Currie, T., & Sicilia-Aguilar, A. 2011, ApJ, 732, 24
Davis, C. J., Matthews, H. E., Ray, T. P., Dent, W. R. F., & Richer, J. S. 1999, MNRAS, 309, 141
Davis, C. J., Scholz, P., Lucas, P., Smith, M. D., & Adamson, A. 2008, MNRAS, 387, 954
Davis, C. J., Gell, R., Khanzadyan, T., Smith, M. D., & Jenness, T. 2010, A&A, 511, A24
Forbrich, J., & Preibisch, T. 2007, A&A, 475, 959
Groppi, C. E., Kulesa, C., Walker, C., & Martin, C. L. 2004, ApJ, 623, 291
Groppi, C. E., Hunter, T. R., Blundell, R., & Sandell, G. 2007, ApJ, 670, 489
Hartigan, P., & Graham, J. A. 1987, AJ, 93, 913
Hartigan, P., & Lada, C. J. 1985, ApJS, 59, 383
Kraus, S., Hofmann, K.-H., Malbet, F., et al. 2009, A&A, 508, 787
Meyer, M. R., & Wilking, B. A. 2009, PASP, 121, 350
Neuhauser, R., & Forbich, J. 2008, in Handbook of Star Forming Regions, Vol. II, ed. B. Reipurth (ASP)
Nisini, B., Antoniucci, S., Giannini, T., & Lorenzetti, D. 2005, A&A, 429, 543
Nutter, D. J., Ward-Thompson, D., & Andre, P. 2005, MNRAS, 357, 975
Peterson, D. E., Garatti, A. C. O., Bourke, T. L., et al. 2011, ApJS, 194, 43
Robitaille, T. P. 2008, in Massive Star Formation: Observations Confront Theory, ed. H. Beuther, H. Linz, & T. Henning, ASP Conf. Ser., 387, 290
Robitaille, T. P., Whitney, B. A., Indebetouw, R., Wood, K., & Denzmore, P. 2006, ApJS, 167, 256
Robitaille, T. P., Whitney, B. A., Indebetouw, R., & Wood, K. 2007, ApJS, 169, 328
Reipurth, B., & Graham, J. A. 1988, A&A, 202, 219
Taylor, K. N. R., & Storey, J. W. V. 1984, MNRAS, 209, 5
Tuthill, P. G., Monnier, J. D., & Danchi, W. C. 2001, Nature, 409, 1012
Walsh, A. J., Myers, P. C., Di Francesco, J., et al. 2007, ApJ, 655, 958
Wang, H., Mundt, R., Henning, T., & Apai, D. 2004, ApJ, 617, 1191
Wilking, B. A., McCaughrean, M. J., Burton, M. G., et al. 1997, AJ, 114, 5

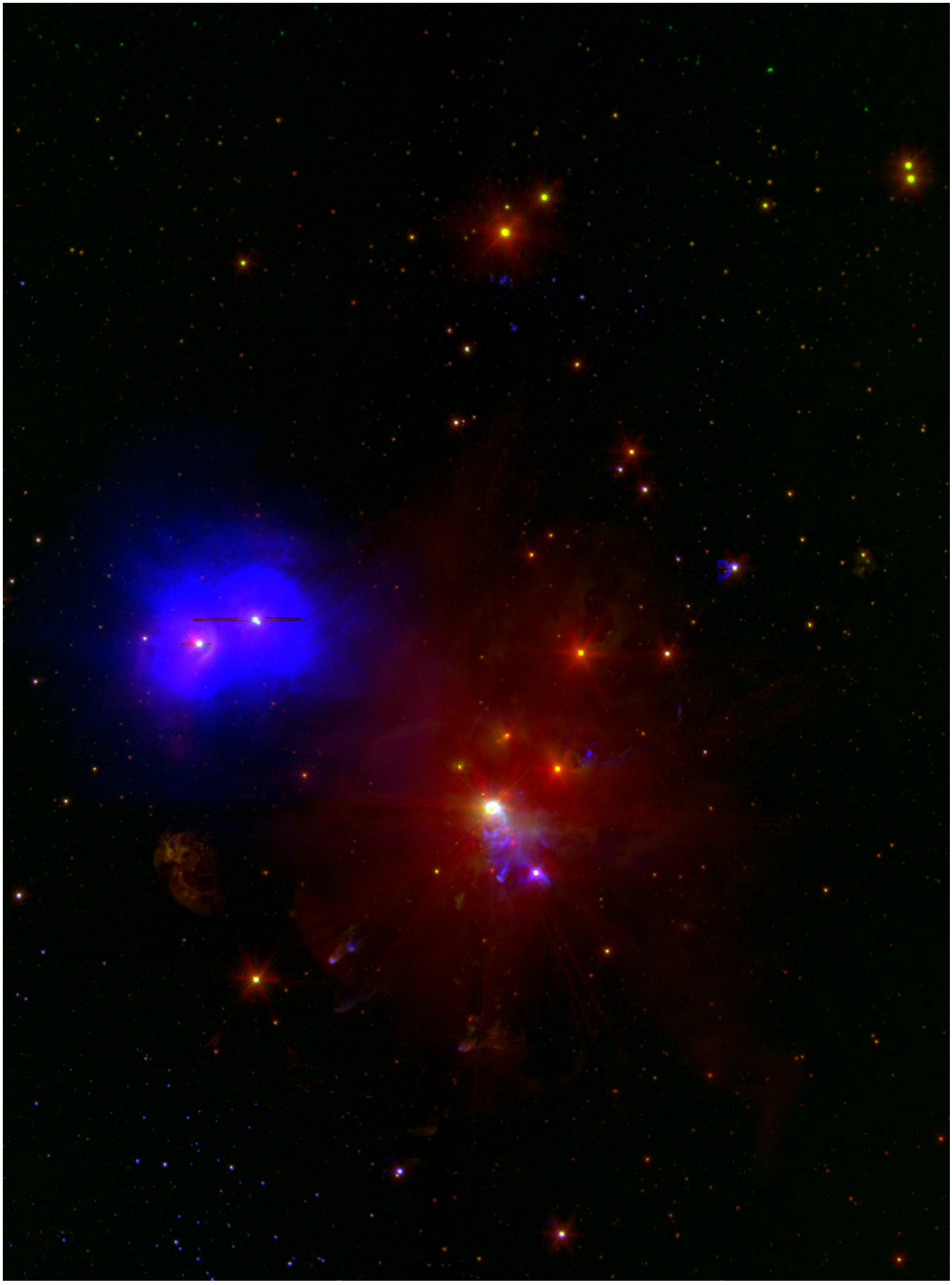

Fig. 1. A coloured image of the region studied in this work. The colour image was obtained by coding *Spitzer* IRAC 4.5 μm image as red, H_2 narrowband image as green and SII image (Wang et al. 2004) as blue. The SII data do not cover the lower portion of the image.